MODEL AND PERFORMANCE ANALYSIS OF COUPLED HEAT AND MOISTURE TRANSFER OF THE ROADBED SLOPE

by

Mingzhe OUYANG [a*], ***Wei WANG*** [a], ***Enhai LIU*** [b*], **and *Wenyun ZHANG*** [b]

[a] School of Civil Engineering, Harbin Institute of Technology, Harbin, China
[b] School of Petroleum Engineering, Changzhou University, Changzhou, China

Original scientific paper
https://doi.org/10.2298/TSCI2203585O

The soil samples of the roadbed slope of the Datong-Xi'an high-speed railway section are taken as the research object. The frost-heave property of the fiber soil of the roadbed slope under a single freeze-thaw cycle is studied, where the fiber's content is taken into account. The distributions of temperature and humidity fields inside the slope are numerically studied, and the coupling transfer of heat and moisture is revealed. The results are helpful for the optimal design of the roadbed slope.

Key words: *coupled heat and moisture, slope, frost-heave amount, fiber content, mechanical properties*

Introduction

In recent years, the roadbed slope protection has been attracted much attention, and high requirement has been put forward for enhancing the railway roadbed and the slope soil. The soil is a porous medium, and its internal heat and moisture transfer significantly affect the stability and service life of the slope. Therefore, many scholars have done a lot of research on a couple of heat and moisture transfers. Tariku *et al.* [1] established a transient model to solve the coupled transmission of heat, gas, and moisture in multilayer porous media. Vasil'ev *et al.* [2] used a 1-D heat and moisture transfer model to reveal the main factors affecting the transfers. Qin *et al.* [3] compared some models, *e.g.*, CTF-conduction transfer function model, the HMT-heat, and moisture combined transmission model, to reveal the advantages and disadvantages of each model. Zhu *et al.* [4] used centrifugal model tests to put forward the deformation, failure characteristics, and failure modes of expansive soil slopes. Zhan *et al.* [5] used in-situ monitoring to study the instability mechanism of expansive soil slopes under different rainfall intensities. To improve the physical and mechanical properties of the soil, fibers were added to soil and concrete [6, 7], which have received extensive attention in recent years. Hu *et al.* [8] studied the variation of cohesion and internal friction of basalt fiber loess with a fiber content based on orthogonal experiments. Li [9] comparatively studied the mechanical properties and crack resistance of four kinds of polyvinyl alcohol fibers mixed with cement. Rose *et al.* [10] studied the influence of various variables on the mechanical properties of dis-

* Corresponding authors, e-mails: mingzhe123456@126.com; liuenhai1018@126.com

crete fiber-reinforced sand samples and found that when the optimal fiber length was 51 mm and the fiber content was 0.6-1.0%, the performance was the best. Han *et al.* [11] obtained the best shear strength when the fiber length and content were 9 mm and 3‰, respectively.

In recent years, theoretical studies have been extremely conducted on the coupled heat and moisture transfer with temperature and relative humidity. However, the logarithmic capillary pressure was ignored, which greatly affects the moisture transfer. Based on the Datong-Xi'an high-speed railway project, this paper investigates the soil samples of the roadbed slopes (184 points, 2-3 m deep) as the research object. From the aspects of soil quality, frost heave effect and construction of roadbed slopes, the paper simulates the distribution of temperature and humidity fields inside the roadbed slopes under three typical climates and explores the coupled transfer of heat and humidity. In order to effectively solve the problems of roadbed slopes soil strength and tensile properties, this paper is to explore the frost heave of the fiber soil under a single freeze-thaw cycle, the different fiber contents, the influence factors of the construction on the slope rain erosion and the slope frost heave.

Theoretical analysis of numerical modeling

Comprehensively considering the various factors affecting the frost heave of the slope in the seasonal freezing zone, the following simplifications and assumptions were made when the heat and moisture transfer in the porous medium filler of the slope were numerically modeled. The heat and moisture migration process in the filler was a 1-D process. The water vapor and air in the slope filler were calculated as ideal gases. There was a heat and moisture balance at the interface of the multilayer filler. There was no phase change process of solidification and melting. According to the energy conservation and mass conservation equations, the heat and moisture transfer equilibrium equation inside the porous medium filler and the relationship change equation between relative humidity and capillary pressure can be obtained from Kelvin relationship [12, 13]:

$$p_c = -\rho_l R_D T \ln(\varphi) \tag{1}$$

where p_c [Pa] is the capillary pressure, ρ_l [kgm^{-3}] – the density of liquid water, R_D [Jkg^{-1}K^{-1}] – the gas constant of water vapor, and φ [%] – the relative humidity.

Jin *et al.* [14] suggested a new theory to explain the capillary pressure. The geometric boundary also plays an essential role in the capillary rise.

According to the definition of relative humidity, the gradient of state variable ∇p_s can be transformed into:

$$\nabla p_s = \frac{\partial p_s}{\partial x} = \frac{\partial \varphi p_{sat}}{\partial x} = \left(\varphi \frac{\partial p_{sat}}{\partial x} + p_{sat}\frac{\partial \varphi}{\partial x}\right) = \left(\varphi \frac{\partial p_{sat}}{\partial T}\frac{\partial T}{\partial x} + p_{sat}\frac{\partial \varphi}{\partial x}\frac{\partial p_c}{\partial x}\right) =$$

$$= \left(\varphi \frac{\partial p_{sat}}{\partial T}\frac{\partial T}{\partial x} - p_{sat}\frac{\varphi}{\rho_l R_D T}\frac{\partial p_c}{\partial L p_c}\frac{\partial L p_c}{\partial x}\right) \tag{2}$$

where $Lp_c = \log_{10}(p_c)$ is the defined logarithmic capillary pressure, p_s [Pa] – the partial pressure of water vapor, p_{sat} [Pa] – the saturated steam pressure, and T [K] – the temperature. Among them, the heat and moisture coupling equilibrium equation with temperature and logarithmic capillary pressure as the driving potential are:

$$(\rho_{\mathrm{m}}c_{p,\mathrm{m}}+\omega c_{p,\mathrm{l}})\frac{\partial T}{\partial t}=\nabla(\lambda\nabla T)+h_{\mathrm{s}}(\nabla\mu_p\nabla p_{\mathrm{s}})+h_{\mathrm{s}}r_{\mathrm{a}}\rho_{\mathrm{s}}\nabla p_{\mathrm{s}}-r_{\mathrm{a}}\rho_{\mathrm{d}}c_{p,\mathrm{d}}\nabla T=$$

$$=\left[\nabla\lambda+h_{\mathrm{s}}(\nabla\mu_p-r_{\mathrm{a}}\rho_{\mathrm{s}})\varphi\frac{\partial p_{\mathrm{sat}}}{\partial T}-r_{\mathrm{a}}\rho_{\mathrm{d}}c_{p,\mathrm{d}}\right]\nabla T+h_{\mathrm{s}}(\nabla\mu_p+r_{\mathrm{a}}\rho_{\mathrm{s}})p_{\mathrm{sat}}\frac{\varphi}{\rho_{\mathrm{l}}R_DT}\frac{\partial p_{\mathrm{c}}}{\partial Lp_{\mathrm{c}}}\nabla Lp_{\mathrm{c}} \quad (3)$$

$$\frac{\partial\omega}{\partial t}=\frac{\partial\omega}{\partial p_{\mathrm{c}}}\frac{\partial p_{\mathrm{c}}}{\partial Lp_{\mathrm{c}}}\frac{\partial Lp_{\mathrm{c}}}{\partial t}=\nabla(j_{\mathrm{s}})-r_{\mathrm{a}}\rho_{\mathrm{s}}\nabla p_{\mathrm{s}}+\nabla(-k_{\mathrm{l}})\nabla p_{\mathrm{c}}=$$

$$=(\nabla\mu_{\mathrm{p}}-r_{\mathrm{a}}\rho_{\mathrm{s}})\varphi\frac{\partial p_{\mathrm{sat}}}{\partial T}\nabla T+\left[(-\nabla\mu_{\mathrm{p}}+r_{\mathrm{a}}\rho_{\mathrm{s}})p_{\mathrm{sat}}\frac{\varphi}{\rho_{\mathrm{l}}R_DT}\frac{\partial p_{\mathrm{c}}}{\partial Lp_{\mathrm{c}}}-\nabla k_{\mathrm{l}}\frac{\partial p_{\mathrm{c}}}{\partial Lp_{\mathrm{c}}}\right]\nabla Lp_{\mathrm{c}} \quad (4)$$

where $j_{\mathrm{s}}=\mu_{\mathrm{p}}\nabla p_{\mathrm{s}}$ [kgm^{-2}s^{-1}] is the diffusion of water vapor, ρ_{m} [kgm^{-3}] – the density of the dry material, $c_{p,\mathrm{m}}$ [Jkg^{-1}K^{-1}] – the specific heat of the dry material, ω [kgm^{-3}] – the volumetric moisture content, $c_{p,\mathrm{l}}$ [Jkg^{-1}K^{-1}] – the specific heat of liquid water, t [s] – the time, λ [Wm^{-1}K^{-1}] – the thermal conductivity, h_{s} [Jkg^{-1}] – the specific enthalpy of water vapor, r_{a} [ms^{-1}] – the flow rate of wet air, ρ_{s} [kgm^{-3}] – the density of water vapor, ρ_{d} [kgm^{-3}] – the density of dry air, $c_{p,\mathrm{d}}$ [Jkg^{-1}K^{-1}] – the specific heat of dry air, μ_{p} [kgm^{-1}s^{-1}Pa^{-1}] – the water vapor permeability coefficient, k_{l} [kgm^{-1}s^{-1}Pa^{-1}] – the liquid water permeability coefficient, and p_{c} [Pa] – the capillary pressure.

Physical model

Parameters and models

According to the roadbed reference materials, the typical section design parameters were used as the basis of the geometric model size. The slope height was 5 m, the upper slope ratio was 1:1.5, the lower slope ratio was 1:1.75, and the shoulder width was 1 m. The fiber soil was symmetrically distributed on both sides of the slope, and the study range was 3 m from the ground surface. The geometric model of the roadbed slope and the distribution of filler were shown in fig. 1.

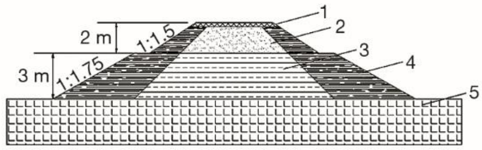

Figure 1. Geometry model and filler distribution diagram;
1 – cement graded gravel, 2 – base layer surface filler, 3 – base layer bottom filler, 4 – fiber soil, 5 – silty clay

Numerical simulation

– The moisture flow through the outer surface of the roadbed slope is:

$$g_m=h_m(\varphi_1 p_{\mathrm{sat},1}-\varphi_2 p_{\mathrm{sat},2}) \quad (5)$$

where h_m [kgm^{-2}s^{-1}Pa^{-1}] is the convective heat transfer coefficient of the outer surface of the slope, φ_1 [%] – the relative humidity of the environment, φ_2 [%] – the relative humidity of the outer surface of the slope, $p_{\mathrm{sat},1}$ [Pa] – the saturated vapor pressure of the environment, and $p_{\mathrm{sat},2}$ [Pa] – the saturated vapor pressure on the outer surface of the slope.

– Simulation used 2-D unsteady state numerical calculation (total duration was 24 hours, starting from 12:00, calculation unit was *h*, using Xi'an meteorological data), through three typical climates, namely summer July, winter January, and transition season (take the average temperature) for simulation.

Temperature distribution of roadbed slope under different climatic conditions

The temperature distribution of roadbed slopes in summer, transition season, and winter were shown in figs. 2-4, respectively.

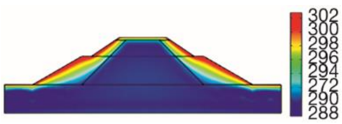

Figure 2.Temperature distribution of roadbed slope in summer

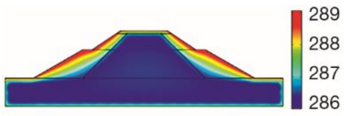

Figure 3.Temperature distribution of roadbed slope in a transition season

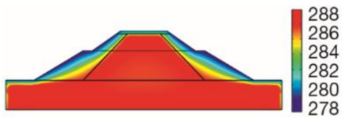

Figure 4.Temperature distribution of roadbed slope in winter

As can be seen in fig. 2, when the summer ambient temperature reached the highest in a year, the outer surface temperature of the slope also reached a maximum of about 29.5 ℃, and the difference between the highest temperature and the lowest temperature was 14.5 ℃. The lowest temperature area was mainly concentrated in the range of base layer bottom filler and silty clay. Comparing the temperature distribution, figs. 2 and 3, it can be seen that as the ambient temperature decreased, the outer surface temperature of the slope also decreased, the temperature range decreased with the increase in depth, and the difference between the internal temperature and the internal temperature was reduced to 3 ℃. Figure 4 showed that the temperature distribution of the roadbed slope in winter was diametrically opposite to the temperature distribution in summer and transition seasons. The main reason for this phenomenon was that the surface temperature decreased to about 3 ℃ with the environment, while the deep soil temperature was higher than the outside, which resulted in the temperature transfer from the inside to the outside. The outer surface temperature was low, and the center temperature was high.

Moisture distribution of roadbed slope under different climatic conditions

The humidity distribution diagrams of roadbed slopes in summer, transition season and winter were shown in figs. 5-7, respectively.

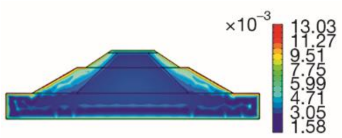

Figure 5. Moisture distribution of roadbed slope in summer

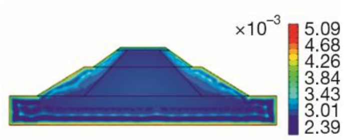

Figure 6. Moisture distribution of roadbed slope in a transition season

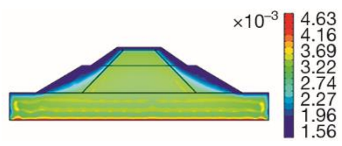

Figure 7. Moisture distribution of roadbed slope in winter

According to fig. 5, the humidity of the surface in direct contact with the ambient air was the highest in summer, and the difference with the lowest humidity area was about $11.5 \cdot 10^{-3}$. Comparing fig. 5 with fig. 6 reveals that after the summer enters the transition season, the humidity of the outer surface of the slope decreases rapidly with the decrease of the ambient temperature and relative humidity, and the humidity of the area below the center of the slope rose slightly. According to fig. 7, the humidity gradient of the roadbed slope in winter was opposite to that of summer and transition seasons. The outer surface of the slope had lower humidity and the center humidity was higher, but the highest humidity value was still higher than the humidity of the outer layer of the slope in the transition season, indicating that the winter humidity value did not change significantly.

Results and analysis

The simulation results showed:

- The temperature and humidity of the 3 m deep roadbed and the slope center from the ground surface under different climatic conditions were relatively stable.
- The temperature gradient and humidity gradient were in the same direction as the water vapor pressure gradient.
- The slope temperature and humidity distribution gradients in winter were opposite to those in summer and transition seasons. Due to the area below the slope center was far from the external environment, the temperature and humidity changes were both significant hysteresis.

Analysis of protection against frost heave of slope filling samples

This paper compared the physical and mechanical properties of fiber soil in the literature [15-17] to analyze the frost heave protection and performance analysis of the roadbed slope fill sample.

Test materials and design

The low-liquid-limit silty clay for the test was selected from the vicinity of Xi'an Railway. According to the geotechnical test specification JGJ/T104-2011, we selected an appropriate amount of clean silty clay, dried it naturally, sieved through a 2 mm sample sieve, and stored it for subsequent test samples of fiber soil. In view of the fact that fresh concrete was affected by frost damage in a low-temperature environment (≤–5 °C), which made hydration difficult. In order to avoid the expansion, deformation and slippage of the cement paste (Harbin Cement P.O 42.5, mortar ratio 1:1, water-cement ratio 0.2, particle diameter 1.18 mm, the experimental temperature –20 °C), and aggregate due to the ice crystal structure, and weaken the bonding force of the concrete, the subsequent test specimens were stripped and weighed, wrapped in a film, placed in a constant temperature and humidity box for seven days, and the temperature and relative humidity were, respectively, controlled at 20 ±2 °C, about 95%. The experiment was designed in six groups, two times in each group, and the experiment results were averaged. The design of digital bridge test sample resistance and temperature control instrument to monitor sample center temperature was shown in figs. 8 and 9, respectively.

Comprehensive protection analysis

Investigating and testing the moisture content of the fill soil samples (particle size less than 30 mm) of the roadbed slope of the Datong-Xi'an high-speed railway section (184 points, 2-3 m deep) before freezing. The probability distribution of water content was in the range of 16.3-26.3%, accounting for 94.7%, and the remaining probability was only 5.3%. With reference to the water content detection of the test slope fill soil samples, it was determined that the variation range of the water content index was 16.3-26.3%, and the roadbed compaction level was mainly distributed between 70% and 85%.

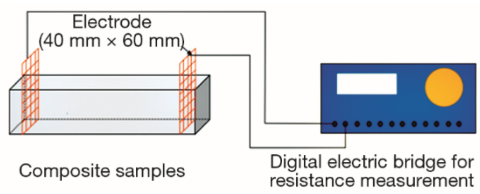

Figure 8. Digital bridge test sample resistance

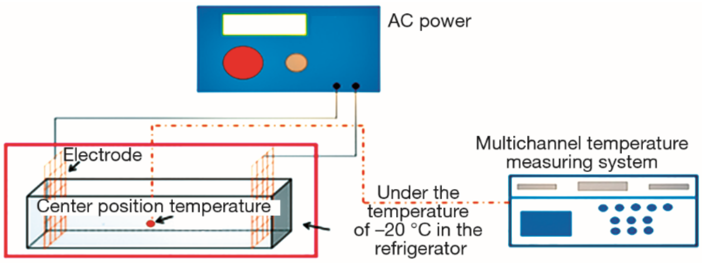

Figure 9. Temperature controller monitors sample center temperature

Performance analysis of slope filling samples

According to [17], combined with the data obtained from the field slope protection test of the Datong-Xi'an high-speed railway section, the test set the sample of the special-shaped fiber soil [15-17], the buried length was 16 cm, the moisture content was 12%, and the compaction degree was 96%, the pores between the special-shaped fiber soil sample and the slope protection soil gradually decreased, and the mutual wrapping and gripping effect were gradually enhanced, and the shear strength was better.

Micro characterization

During the test, a SEM was used to observe the microscopic characteristics of the fiber dispersion and anchorage, the pores of the sample matrix, and the aggregation state of sample hydration products inside the sample concrete mortar. The situation of fiber dispersion and anchoring inside the concrete mortar was shown in fig. 10.

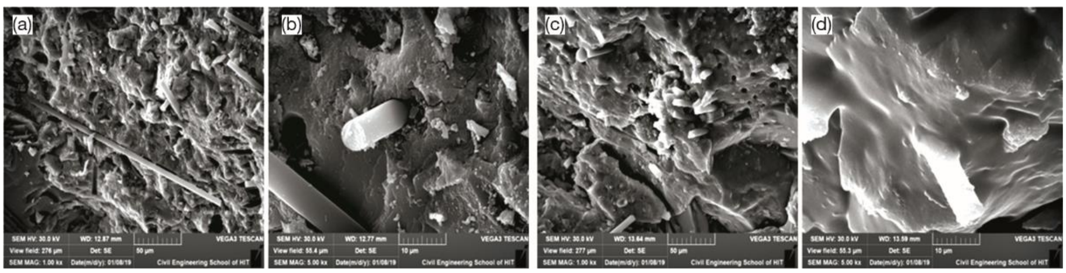

Figure 10. Fiber dispersion and anchorage inside a concrete mortar; (a) standard curing (1000 times), (b) standard curing (5000 times), (c) steam curing (1000 times), and (d) steam curing (5000 times)

According to fig. 10, during the curing process of the sample, the concrete mortar fiber anchorage had a greater impact on the degree of cement hydration of the concrete sample, the curing and crushing treatment of the cement mortar sample, and the fiber composite conductive material in the concrete was preset to construct a conductive path can effectively ensure the conductive stability of the heating process. In the standard curing process of the sample, there were pores on the interface between the blended fiber and the cement mortar hydration gel, which was not conducive to the subsequent anchoring. In the steam curing process, the anchoring degree was significantly better than the standard curing process. The interface between the blended fiber and the hydrated gel was small and the surface was relatively uniform and dense.

Performance analysis

Test samples of special-shaped fiber soil (water content 12%, compaction degree 96%, water-cement ratio 0.32) were used to study the frost heave changes of soil with different fiber content (0‰, 1.5‰, 3‰, 4.5‰, 6‰, and 7.5‰). The influence of different fiber content on the frost heave of the slope fill sample was shown in figs. 11 and 12.

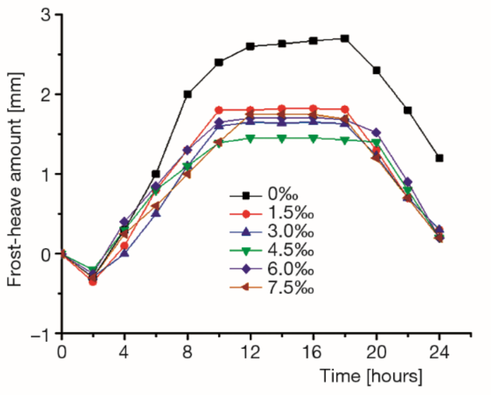

Figure 11. The influence of different fiber content on frost-heave amount

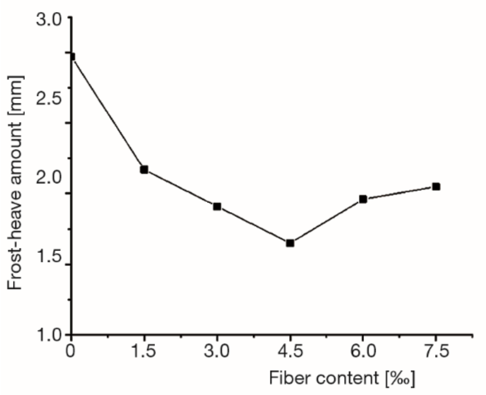

Figure 12. The influence of different fiber content on the maximum frost-heave amount

According to fig. 11, under the conditions of the same degree of compaction, moisture content, and fiber length, increased the fiber content can significantly reduced the amount of frost heave of the soil. The frost-heave amount with different fiber content increased first and then remained with the increase of freezing time, and then decreased rapidly after reaching a certain time. The fiber could be significantly improved the frost heave resistance of the soil body because the fiber and the soil body formed an interweaving effect and then increased the cohesion of the soil body. At the same time, the addition of the fiber made the soil body have a greater capillary water pressure, which made the cohesion force further improved. However, too much fiber content would lead to uneven distribution of soil, resulting in increasing frost heave. According to fig. 12, within a certain range, the amount of frost heave decreased with the increase of fiber content. When the fiber content was 4.5‰, the minimum frost heave was 1.65 mm, and when the fiber content exceeded 4.5‰, the increase of fiber content would cause the increase of frost heave. Therefore, it could be obtained from the test results that when the fiber content was 4.5‰, its frost heave resistance was the best.

Discussion and conclusion

Comprehensively comparing the fiber strength and its bonding force showed that the slope protection soil depends upon many factors including moisture fiber's content. As the studied soil is a porous medium, the fractal theory [18-20] can adopted for future research.

Acknowledgment

This project was supported by the Science and Technology Project of Changzhou City (CE20212045) and National Key Research and Development Plan Fund Project (No. 2017YFC0703500) of China.

References

[1] Tariku, F., *et al.*, Transient Model for Coupled Heat, Air and Moisture Transfer through Multilayered Porous Media, *International Journal of Heat and Mass Transfer, 53* (2010), 15, pp. 3035-3044
[2] Vasil'ev, G. P., *et al.*, Numerical Modeling of Heat and Moisture Diffusion in Porous Materials, *Computational Mathematics and Modeling, 26* (2015), 4, pp. 501-513
[3] Qin, M. H., *et al.*, Evaluation of Different Thermal Models in Energy Plus for Calculating Moisture Effects on Building Energy Consumption in Different Climate Conditions, *Building Simulation, 9* (2016), 1, pp. 15-25
[4] Zhu, X., *et al.*, Failure Modes and Slope Stability of Expansive Soil Canal under Wet-Dry Cycles, *Transactions of the Chinese Society of Agricultural Engineering, 36* (2020), 4, pp. 159-167
[5] Zhan, L. T., *et al.*, Artificial Rainfall Infiltration Tests on a Well-Instrumented Unsaturated Expansive Soil Slope, *Rock and Soil Mechanics, 24* (2003), 2, pp. 151-158
[6] Tang, C. S., *et al.*, Interfacial Shear Strength of Fiber Reinforced Soil, *Geotextiles & Geomembranes, 28* (2010), 1, pp. 54-62
[7] Tang, C. S., *et al.*, Desiccation Cracking Behavior of Polypropylene Fiber-Reinforced Clayey Soil, *Canadian Geotechnical Journal, 49* (2012), 9, pp. 1088-1101
[8] Hu, W. L., *et al.*, Experimental Study on Optimization of Shear Strength Parameters of Basalt Fiber Loess, *The Chinese Journal of Geological Hazard and Control, 30* (2019), 4, pp. 92-97
[9] Li, C. X., Reinforcing Performance of Cement-Stabilized Aggregated Mixture by Polyvinyl Alcohol (PVA) Fiber, *Journal of Transport Science and Engineering, 34* (2018), 1, pp. 19-22,49
[10] Rose, L. S., *et al.*, Engineering Properties of Sand-Fiber Mixtures for Road Construction, *Journal of Geotechnical and Geoenvironmental Engineering, 127* (2001), 3, pp. 258-268
[11] Han, C. P., *et al.*, Experimental Study on Factors of Shear Strength of Fiber Soils under the Freeze-Thaw Cycle, *Journal of Railway Science and Engineering, 12* (2015), 2, pp. 275-281
[12] Belleudy, C., *et al.*, Experimental and Numerical Investigations of the Effects of Air Leakage on Temperature and Moisture Fields in Porous Insulation, *Building & Environment, 94* (2015), Dec. pp. 457-466
[13] Belleudy, C., *et al.*, A 2D Model for Coupled Heat, Air, and Moisture Transfer through Porous Media in Contact with Air Channels, *International Journal of Heat & Mass Transfer, 95* (2016), Apr., pp. 453-465
[14] Jin, X., *et al.*, Low Frequency of a Deforming Capillary Vibration, Part 1: Mathematical Model, *Journal of Low Frequency Noise Vibration and Active Control, 38* (2019), 3-4, pp. 1676-1680
[15] Du, X. Y., *et al.*, Experimental Study on the Physical and Mechanical Properties of Fiber Soil, *Proceedings, the 2017 Annual Conference of China Civil Engineering Society* (2017), 10, pp. 564-575
[16] Ouyang, M. Z., Research on the Protection Technology of Synthetic Resin Fiber in the Slope of Railway Subgrade, M. Sc. thesis, Harbin Institute of Technology, Harbin, China, 2017
[17] Wang, Z. Y., *et al.*, Electro-Thermal Properties and Seebeck-Effect of Conductive Mortar and Its Use in Self-Heating and Self-Sensing System, *Ceramics International, 43* (2017), 12, pp. 8685-8693
[18] Tian, D., *et al.*, Hall-Petch Effect and Inverse Hall-Petch Effect: a Fractal Unification, *Fractals, 26* (2018), 6, ID 1850083
[19] Wang, Y. Y., *et al.*, A Model for the Effective Thermal Conductivity of Moist Porous Building Materials Based on Fractal Theory, *International Journal of Heat and Mass Transfer, 125* (2018), Oct., pp. 387-399
[20] Li, X. X., He, J.-H., Along the Evolution Process: Kleiber's 3/4 Law Makes way for Rubner's Surface Law: A Fractal Approach, *Fractals, 27* (2019), 2, ID 1950015

Paper submitted: August 3, 2020
Paper revised: March 18, 2021
Paper accepted: March 18, 2021